Strojniški vestnik - Journal of Mechanical Engineering 70(2024)7-8, 355-368
DOI:10.5545/sv-jme.2023.885
Original Scientific Paper
Received for review: 2023-11-28
Received revised form: 2024-05-07
Accepted for publication: 2024-07-03

Surface Roughness Evaluation of AZ31B Magnesium Alloy After Rough Milling Using Tools with Different Geometries

Ireneusz Zagórski*
Faculty of Mechanical Engineering, Lublin University of Technology, Poland

This paper presents the experimental results of a study investigating the impact of machining parameters on 3D surface roughness after rough, dry milling. The following 3D roughness parameters were analysed: Sa (arithmetic mean height), Sq (root mean square height), Sz (maximum height), Sku (kurtosis), Ssk (skewness), Sp (maximum peak height), and Sv (maximum pit height). Roughness measurements were made on the end face of the specimens. Additionally, 3D surface topography maps and Abbot-Firestone material ratio curves were generated. Carbide end mills with variable rake and helix angles were used in the study. Experiments were conducted on AZ31B magnesium alloy specimens using a contact-type profilometer. The machining process was conducted using the parameters of so-called high-speed machining. Three variable technological parameters were analysed: cutting speed v_c, feed per tooth f_z, and axial depth of cut a_p. The results showed that the surface roughness of the rough-milled specimens depended to a great extent on the tool geometry and applied machining parameters. Feed per tooth was found to have the greatest impact on surface roughness parameters. Lower values of the analysed surface roughness parameters (and therefore higher surface quality) were obtained (in most cases) for the tools with a rake angle γ of 5° and a helix angle λ_s of 50°. The results provided both theoretical and practical knowledge about the achievable surface roughness after rough milling using tools with different tool blade geometry. It was shown that rough milling is an effective and efficient type of machining for the AZ31B alloy.

Keywords: rough milling, 3D surface roughness, Abbott-Firestone curve, rake angle, helix angle, magnesium alloy

Highlights

- *Rough milling of magnesium alloy AZ31B is an effective and efficient type of machining.*
- *Machined surface roughness depends to a large extent on the geometry of a machining tool.*
- *The change of selected technological parameters (in particular feed per tooth) significantly influences the surface roughness parameters.*
- *Texture and shape of machining marks are typical of rough milling (heterogeneous structure).*
- *Abbott-Firestone curves have a proportional or a degressive-progressive shape.*

0 INTRODUCTION

Among modern construction materials, one can distinguish a group of promising yet insufficiently studied light alloys [1], including aluminium and magnesium alloys. Magnesium alloys are construction materials characterized by low density yet quite high strength. Everyday devices and elements made of AZ91D/HP or AZ31B alloy are widely used in the automotive, aircraft, medical, and sports industries. Machinery and equipment components made of these alloys must meet stringent quality requirements, especially in terms of surface roughness [2]. Regarding surface roughness parameters, the best-explored and most widely studied is the two-dimensional (2D) surface roughness parameter *Ra* (arithmetical mean deviation) [3]. Nevertheless, analyses based on only one roughness parameter seem far from being exhaustive; therefore, other surface roughness parameters must be taken into consideration [4]. In addition to the widely studied 2D parameters, 3D surface roughness parameters can also be investigated in combination with surface topography maps [5] and [6].

Surface roughness is the main machinability indicator of its quality in rough and finish machining [7] and [8], as well as in other new methods and types of machining, including precision machining [9].

Studies have also been conducted on the machinability of different grades of magnesium alloys (e.g., AM60) using carbide tools with different types of tool coatings, e.g. made of TiN [10], where the surface roughness was estimated to be approx. $Ra \approx 0.3$ μm. A study conducted with TiAlN-coated end mills [11] investigated a substantially greater number of surface roughness parameters such as *Rv*, *Rp*, *Rt*, *Ra*, *Rku*, *Rsk*, *RSm*, as well as *Sv*, *Sp*, *St*, *Sa*, *Ssk*, and *Sku* on the lateral and the end face of the specimen. The machinability of AZ61 was investigated, and the obtained *Ra* parameter was in the range of 0.1 μm to 0.4 μm [12]. Another study [13] examined the *Sa* parameter in machining AZ61 alloy for the reversed and direct feed. The obtained *Sa* values ranged from approximately 0.2 μm to 0.8 μm.

*Corr. Author's Address: Faculty of Mechanical Engineering, Lublin University of Technology, Poland, i.zagorski@pollub.pl

The most widely used alloy in practice and investigated in research studies is AZ91D. In a study [14] on high-speed machining, the obtained *Ra* value was from about 0.06 µm to 0.13 µm. Another study [15] showed that the *Ra* parameter increased with v_c and f_z, ranging from 0.4 µm to 1.2 µm. Other studies [16] and [17] investigated the optimization of machining parameters (v_c, f_z, a_p) and the obtained *Ra* value ranged from approximately 0.07 µm to 0.21 µm. A more comprehensive analysis and, thus, the results for a greater number of roughness parameters were reported in [11], which considered both 2D and 3D surface roughness parameters, as well as surface topography maps. Although the AZ91D alloy is usually processed under dry machining conditions, studies have been conducted with the use of MQL or cryogenic conditions [18] and [19].

Another widely used albeit less popular alloy (probably due to its cost) is AZ31B. Components of this alloy grade are often produced from solid material; therefore, the finish allowance is quite substantial, posing the need for machining and machining process analysis [20]. For example, in a study [21], the variation in v_c and f_z yielded a *Ra* value below 0.2 µm. The machining process was conducted by dry cutting with an air coolant. A study [22] compared wet and cryogenic machining. The obtained *Ra* parameter was lower than 1 µm, with approx. 20 % lower *Ra* for cryogenic conditions.

Alloys with alloying elements such as zirconium, rare earths, zinc (e.g., ZE41) or lithium are only used in exceptional cases. These alloys are very expensive and are only used to produce aircraft components, if not primarily for the aerospace industry. For example, a study [23] investigating the milling of ZE41 magnesium alloy showed that *Ra* ranged from approximately 1.4 µm to 4.1 µm, and that increase in v_c and f_z caused the *Ra* parameter to increase too. A similar study [24] demonstrated that the *Ra* parameter value could range from approx. 0.3 µm to 0.7 µm (for variable f_z and a_p).

An interesting group of materials includes alloys containing *Ca* used in medical applications [25] to [29]. The Mg-Ca0.8 alloy was investigated, among others, in [25] to [27], where the obtained *Ra* value ranged from 0.2 µm to 0.8 µm. For this case, however, the machining process was conducted using a tool with a polycrystalline diamond (PCD) edge. In a study [28], depending on the machining strategy employed, the *Ra* values ranged from 0.9 µm to 1.4 µm (normal milling) and 0.09 µm to 0.8 µm (inverse milling). The machining of a similar alloy, Mg-Ca1.0, yielded the *Ra* parameter ranging from 0.10 µm to 0.16 µm [29].

In addition to using 2D and 3D parameters, surface quality can also be evaluated using the Abbott-Firestone curve [11] and parameters describing it. As a result, a different approach to surface quality and texture evaluation can be adopted, particularly in terms of assessing the quality of a surface machined by different methods [30]. Depending on the roughness profile shape, one can distinguish the following curve patterns: progressive, proportional, degressive, and combined (e.g., degressive-progressive, progressive-degressive, proportional-degressive, etc.). Based on the curve shape and selected parameters (*Rpk, Rvk, Rk*), one can make inferences about the tribological resistance of a material [31]. For example, a progressive shape means that the surface is more wear-resistant (rounded peaks of the surface) [32].

As mentioned, previous studies investigating the problem of surface quality usually focus on one 2D surface roughness parameter, i.e. *Ra*. However, this approach is far from being exhaustive due to the many 2D and 3D roughness parameters that can be used to describe machined surface roughness. Moreover, it seems interesting to raise the issue related to the roughness of the machined surface obtained in the milling process for both practical and cognitive reasons. The quality and roughness of the final surface obtained are very important during the production of various types of machine and device elements. The aim is to ensure that the milling process allows for achieving high-quality surfaces without the need, for example, for finish grinding. In turn, the Abbott-Firestone curve analysis complements and extends research related to the quality of the machined surface. This analysis may be important due to the maintenance characteristics of the surface. A progressive shape (the surface is more wear-resistant) is considered favourable for the A-F curves. The primary objective of this study is to gain insight into a machining process for AZ31B alloy and to determine the effect of machining parameters and tool geometry on 3D Surface roughness. In the study, 3D surface roughness parameters such as *Sa*, *Sz*, *Sq*, *Sku*, *Ssk*, *Sp*, and *Sv* are investigated. In addition, examples of both Abbott-Firestone material ratio curves and 3D surface topography maps are given.

The novelty of the study lies in a comprehensive approach to examining the influence of tool geometry, in particular the rake and helix angle, on 3D roughness parameters in dry milling of magnesium alloys. This study provides new information on key aspects of the cutting process, offering practical tips for selecting the machining parameters for increased machining efficiency. The presented research is an extension of

the analyses conducted so far, including the analysis of 2D roughness parameters and selected surface roughness profiles. The novelty of the research is the use of tools with different toll edge geometry, which is the result of many scientific studies conducted at the author's research centre. These studies consider not only technical aspects such as roughness values and tool geometry but also process effectiveness. Also, taking into account the analysis of the impact of various technological parameters, such as cutting speed, feed per tooth, or axial depth of cut, on roughness parameters allows the identification of selected machining conditions, the best due to the quality of the machining and increasing the efficiency of the process.

1 METHODS AND EXPERIMENTAL

The study was performed on specimens of AZ31B alloy. This grade of material is suitable for forming processes. The main application of the AZ31B alloy is the aviation industry; this alloy can also be used in the automotive and electronics industries. In the aviation industry, the AZ31B alloy is manufactured, for example, cockpit and door panels, aircraft hubs and levers, brackets and gearbox housings. Experiments

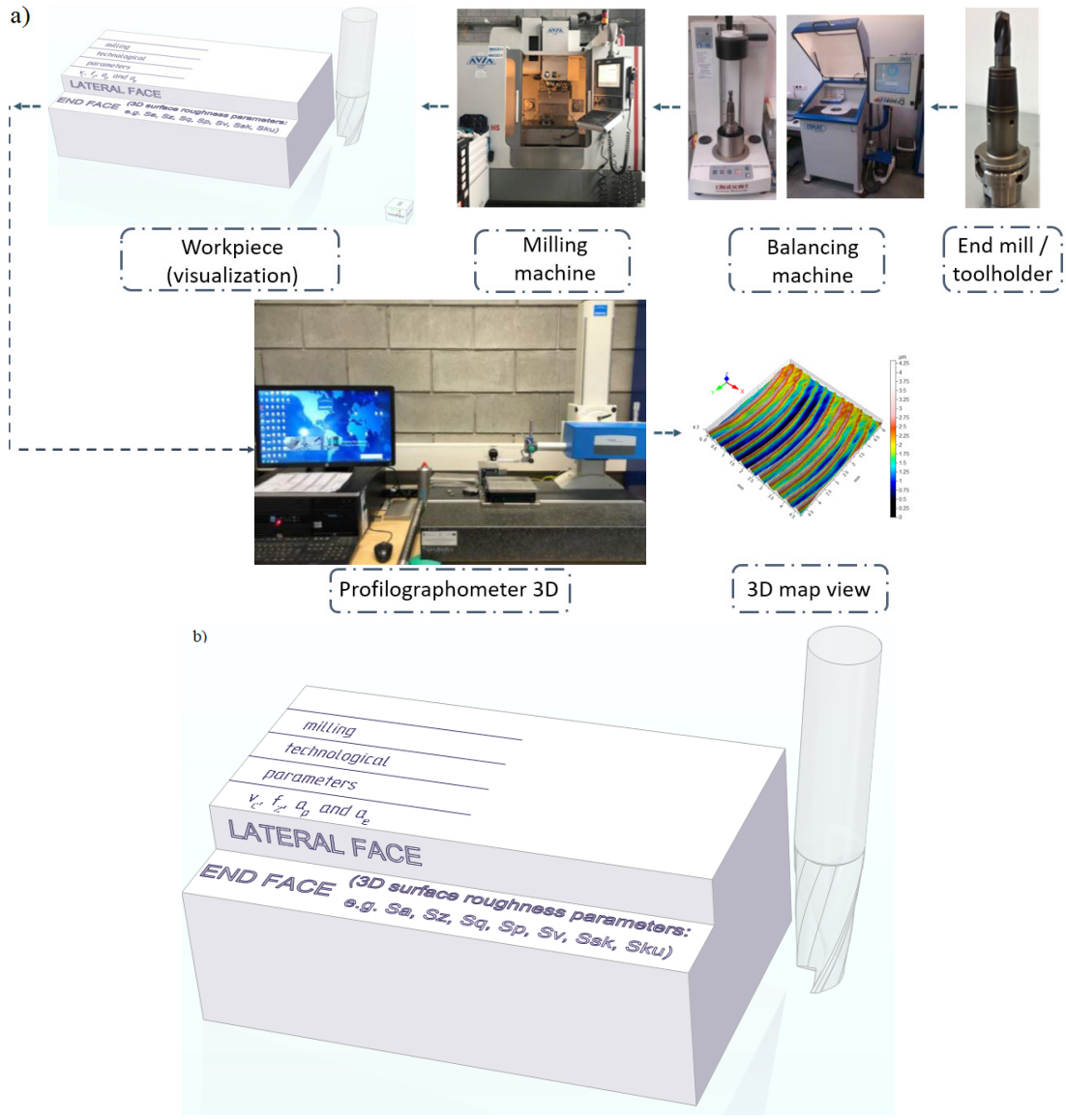

Fig. 1. *Research schematic: a) measuring equipment (e.g. end mill, milling machine and profilometer), and b) milling visualization with a 3D roughness measurement model for the end face on the workpiece*

were conducted under dry, rough milling conditions. Variable technological parameters of milling and different tool geometry were used. The experiments were conducted using carbide end mills (the number of blades $z = 3$) with variable rake angle ($\gamma = 5°$, $\gamma = 30°$) and helix angle ($\lambda_s = 20°$, $\lambda_s = 50°$). Milling was conducted as a high-speed machining process. The tools had a diameter of 16 mm. Milling was conducted on the vertical machining centre AVIA VMC800HS. The employed research structure is shown in Fig. 1.

The end mills with variable geometry were mounted in heat-shrinking tool holders. The holder-tool system was balanced at G2.5 with a balancing machine CIMAT RT 610 in compliance with the ISO 21940–11:2016 standard **[33]**.

The following technological parameters of milling were applied, as shown in Table 1.

Table 1. *Milling technological parameters*

End mill	v_c [m/min]	f_z [mm/tooth]	a_p [μm]	a_e [mm]
$\gamma = 5°$	400	0.15	6.0	14
	1200			
$\gamma = 30°$ $\lambda_s = 20°$	800	0.05	6.0	
		0.30		
$\lambda_s = 50°$	800	0.15	0.5	
			6.0	

The following 3D roughness parameters were analysed: *Sa*, *Sq*, *Sz*, *Sku*, *Ssk*, *Sp*, and *Sv*. Additionally, selected 3D surface topography maps and Abbot-Firestone curves were generated. All surface roughness measurements were made on the end face of the specimen using a contact-type profilometer, Hommel Etamic T8000 RC120-400. The 3D roughness parameters were measured in the direction perpendicular to the machining marks. The scanning area was 4.8 mm × 4.8 mm with 100 scanning steps.

2 RESULTS AND DISCUSSION

This section presents the experimental results of 3D surface roughness evaluation for AZ31B magnesium alloy. The results are described in two separate subsections, depending on the tool blade geometry. The effects of variable rake angle γ (Subsection 2.1) and variable helix angle λ_s (Subsection 2.2) are discussed separately. Moreover, the impact of variations in the technological parameters of milling, i.e., v_c, f_z, a_p, is analysed. In addition to that, selected 3D surface topography maps (Subsection 2.3) of the machined surface roughness and Abbott-Firestone (A-F) curves (Subsection 2.4) are presented.

2.1 Various Rake Angle γ Versus Roughness Parameters

Fig. 2 shows the results of 3D surface roughness parameters for variable cutting speeds and different rake angles.

It can be observed that the type of tool, and particularly its rake angle, has a considerably significant effect on surface roughness. Smaller values of the 3D surface roughness parameters *Sa*, *Sq*, *Sz*, *Sv*, and *Sp* were obtained when the tool with a smaller rake angle (γ of 5°) was used. This observation is quite interesting because references often recommend that light alloys, including magnesium alloys, should be machined using tools with the sharpest possible blade geometry. The term "tools with the sharpest possible blade geometry" should mean the values of the rake angle, clearance angle, and helix angle should be as large as possible. Common recommendations regarding the values angles of the end mill are rake angle in the range of 15° to 25°, clearance angle in the range of 12° to 20°, and helix angle in the range of 30° to 40°. For this case, however, the use of the tool with a smaller rake angle made it possible to obtain a surface of higher quality and, thus, with lower values of the analysed 3D surface roughness parameters.

An analysis of the Ssk parameter reveals that for lower cutting speeds this parameter takes negative values, which may indicate a higher frequency of deep valleys (defined as a plateau and considered optimal). The symmetric distribution of the profile is reflected by zero skewness (this value is similar to that obtained with v_c 1200 and γ 30°). Moreover, the Rsk/Ssk parameter can be used to, e.g., enhance lubrication and support technological process analysis because surfaces with positive skewness show good adhesion resistance. As for Sku, lower values of kurtosis were obtained with higher cutting speed and sharper tool geometry. It is generally assumed that high values of Rku indicate the presence of sharp peaks and grooves (above 3), while the values below 3 indicate that the peaks and grooves are rounded. A study **[32]** showed that without lubrication, the surfaces with positive Rsk and high Rku should result in a lower static friction coefficient compared to the surfaces with Rsk = 0 and Rku = 3.

Fig. 3 shows the results of 3D surface roughness parameters for variable feed per tooth and different rake angles.

The parameters *Sa*, *Sq*, *Sp*, and *Sv* depend on variations in feed per tooth and rake angle. An increase in feed per tooth considerably impacts the analysed surface roughness parameters. The use of higher rake angle results in increased values of *Sa*, *Sq*, *Sp*, and *Sv*,

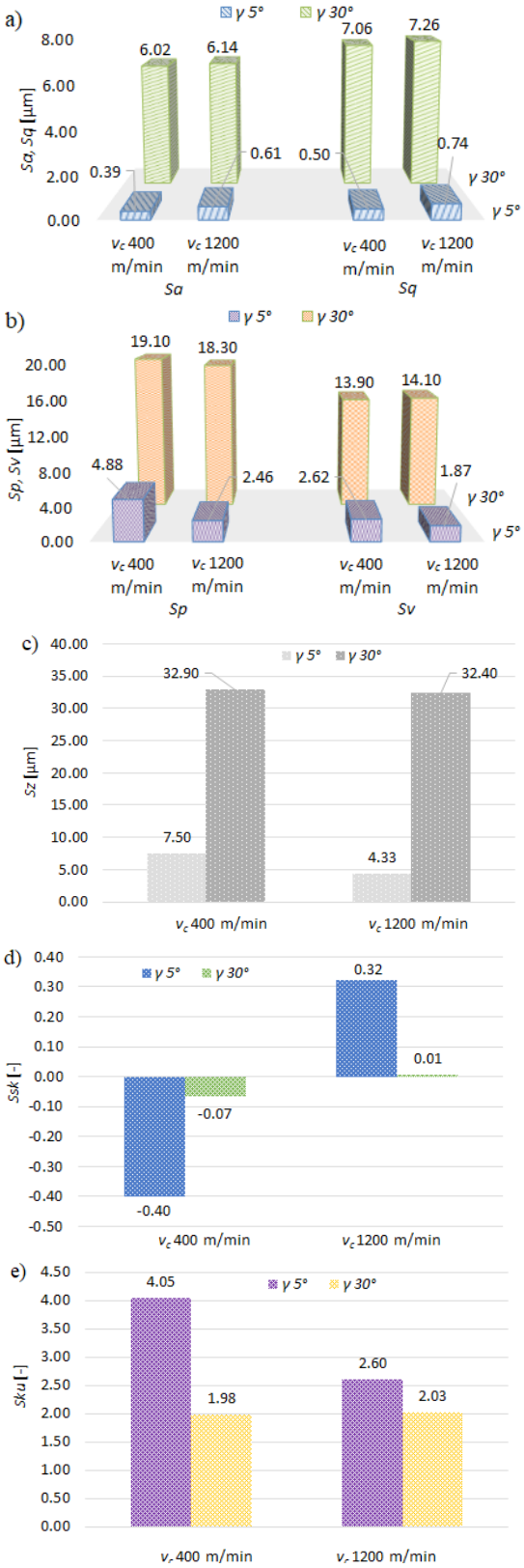

Fig. 2. *Cutting speed and rake angle versus 3D surface roughness parameters: a) Sa, Sq, b) Sp, Sv, c) Sz, d) Ssk, e) Sku*

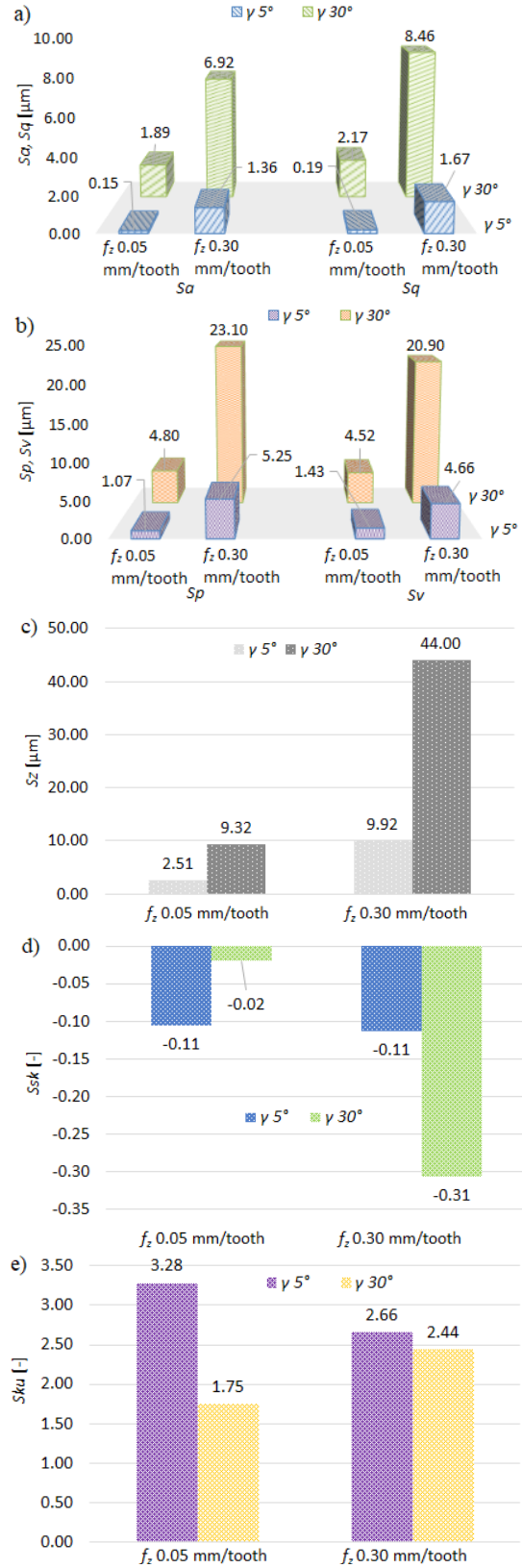

Fig. 3. Feed per tooth and rake angle versus 3D surface roughness parameters: *a) Sa, Sq, b) Sp, Sv, c) Sz, d) Ssk, e) Sku*

this increase being approx. by 4 to 5 times. It can be observed that a further increase in feed per tooth and rake angle also has an impact on the other analysed 3D surface roughness parameters. For Sz, this increase is substantial (approx. by 4 to 5 times) due to a higher cut layer section. The *Sz* values are higher for the tool with a higher rake angle (sharper geometry).

An analysis of the parameters *Ssk* and *Sku* reveals two trends. The *Ssk* parameter takes negative values (a higher frequency of valleys and hence of a surface defined as a plateau, considered optimal). However, for the milling process conducted with f_z 0.05 and γ 30°, the skewness is about zero, and the profile has a symmetric distribution. The *Sku* parameter takes only positive values. Similarly to the case with variable v_c, lower kurtosis values were obtained for a tool with sharper geometry (γ 30°).

Fig. 4 shows the results of 3D surface roughness parameters for variable axial depth of cut and different rake angles.

An opposite trend can be observed when the milling process is conducted with a variable axial depth of cut. Specifically, the 3D surface roughness parameters (*Sa*, *Sq*, *Sp*, *Sv*, *Sz*) are lower (for higher a_p), particularly for the tool with a rake angle of 30°. An increase in the rake angle results in an increase in the values of these parameters. This situation is analogous to that observed for variable cutting speed and feed per tooth.

An analysis of the relationship between variations in axial depth of cut and rake angle and the *Ssk* and *Sku* parameters demonstrates that all obtained values are positive (even though for γ 5° and a_p 6.0 mm, the *Ssk* value is close to zero, amounting to 0.02; a symmetric distribution of the profile is reflected by zero skewness). The positive skewness value may indicate a higher frequency of sharp peaks. The positive high values of kurtosis indicate the presence of sharp peaks and grooves (above 3). For a_p equal to 0.5 mm, the results obtained with both tools are similar, while for ap of 6.0 mm, the *Sku* value is lower for the γ 30° tool.

2.2 Various Helix Angle λs Versus Roughness Parameters

Fig. 5 shows the results of 3D surface roughness parameters for variable cutting speeds and different helix angles.

Considering the tools with various helix angles, the analysed 3D surface roughness parameters (*Sa*, *Sq*, *Sp*, *Sv*, *Sz*) are higher for a helix angle of 20°. An increase in cutting speed leads to an increase in the surface roughness parameters *Sa* and *Sq*. The trend for

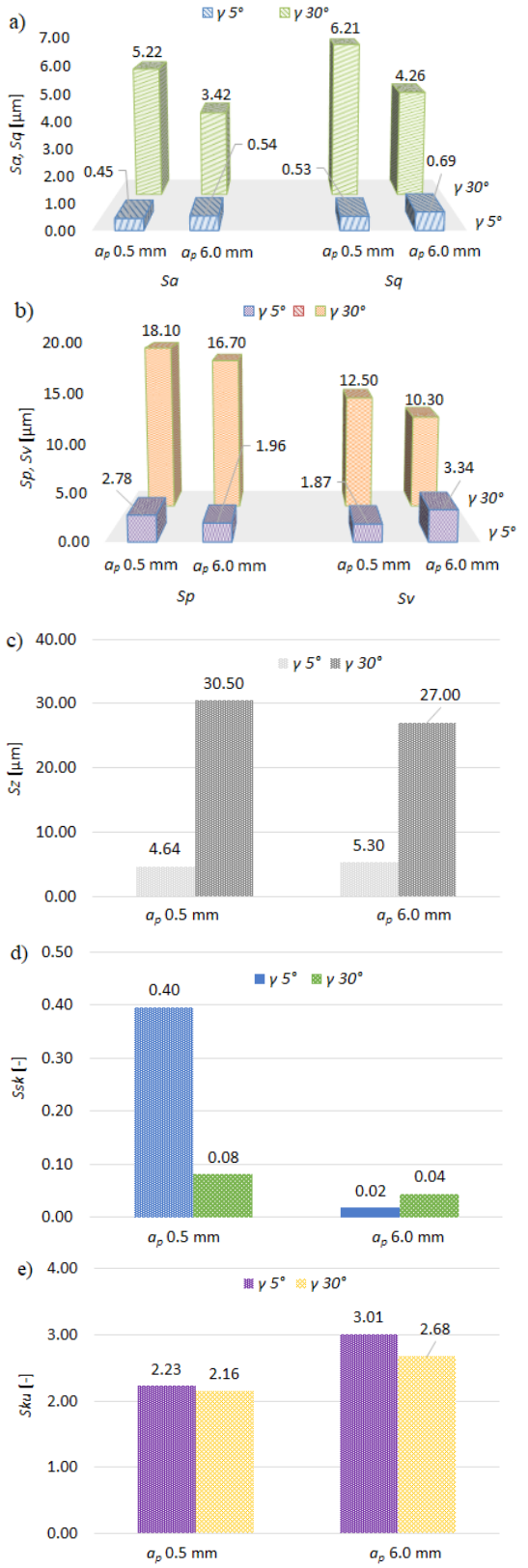

Fig. 4. *Axial depth of cut and rake angle versus 3D surface roughness parameters: a) Sa, Sq, b) Sp, Sv, c) Sz, d) Ssk, e) Sku*

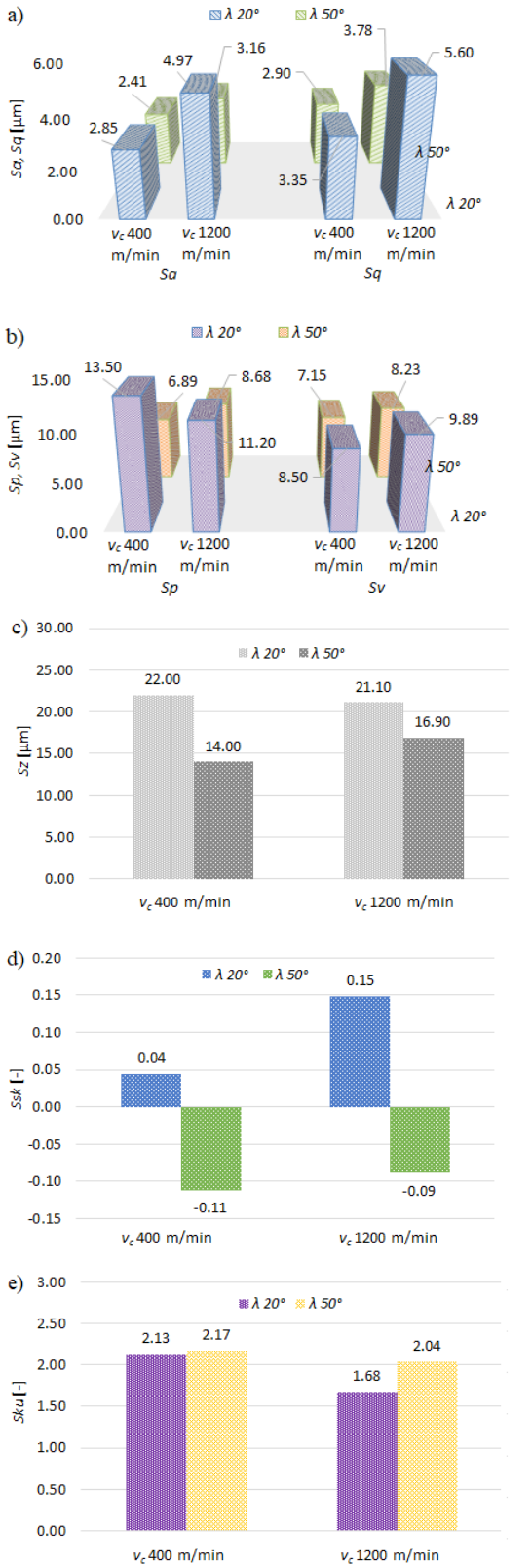

Fig. 5. *Cutting speed and helix angle versus 3D surface roughness parameters: a) Sa, Sq, b) Sp, Sv, c) Sz, d) Ssk, e) Sku*

the parameters *Sa* and *Sv* is similar to that observed for Sa and Sq; however, when the milling process is conducted with a helix angle of 20°, an opposite trend is observed for the *Sp* parameter.

It can be observed that for the tool with a helix angle of 20°, the *Ssk* parameter is positive, and its value increases with an increase in cutting speed, whereas for the tool with a helix angle of 50° the *Ssk* parameter takes a negative value which decreases with an increase in cutting speed. The *Sku* parameter takes only positive values. The kurtosis values below 3 indicate that the peaks and grooves are rounded.

Fig. 6 shows the results of 3D surface roughness parameters for variable feed per tooth and different helix angles.

An analysis of the effect of feed per tooth on the parameters *Sa*, *Sq*, *Sp*, and *Sv* reveals that the surface roughness parameters increase with feed per tooth. An increase in helix angle causes a decrease in *Sa* when the feed per tooth is 0.05 mm/tooth. An opposite situation can be observed when the feed per tooth is equal to 0.30 mm/tooth. The value of *Sv* and *Sp* decreases with increasing helix angle; however, when the feed per tooth is 0.30 mm/tooth, an opposite trend can be observed as the *Sv* parameter value increases.

As for *Sz*, this surface roughness parameter increases with an increase in feed per tooth.

The skewness parameter takes positive values when the feed per tooth is equal to 0.05 mm/tooth. The skewness value is close to zero when the feed per tooth is 0.30 mm/tooth, and the helix angle is 20°. The *Ssk* parameter value is negative when the feed per tooth is 0.30 mm/tooth and the helix angle is 50°. A consistent trend can be observed for kurtosis, where an increase in helix angle causes an increase in *Sku*. The use of a higher feed per tooth causes an increase in *Sku* for a helix angle of 20° and a decrease in *Sku* when the helix angle is equal to 50°.

Fig. 7 shows the results of 3D surface roughness parameters for variable axial depth of cut and different helix angles.

With the axial depth of the cut varying, two opposite trends can be observed. For the end mill with a helix angle of 20°, the use of a higher a_p causes an increase in *Sa* and *Sq*. The same situation can be observed for λ_s 20° and Sv. A different observation can be made when the helix angle is equal to 50°. Both *Sa*, *Sq* and *Sv*, *Sp* decrease with increasing axial depth of cut. A similar situation can be observed for a helix angle of 20° and the *Sp* parameter. For a lower axial depth of cut, the *Sz* value is higher when the milling process is conducted using the tools with

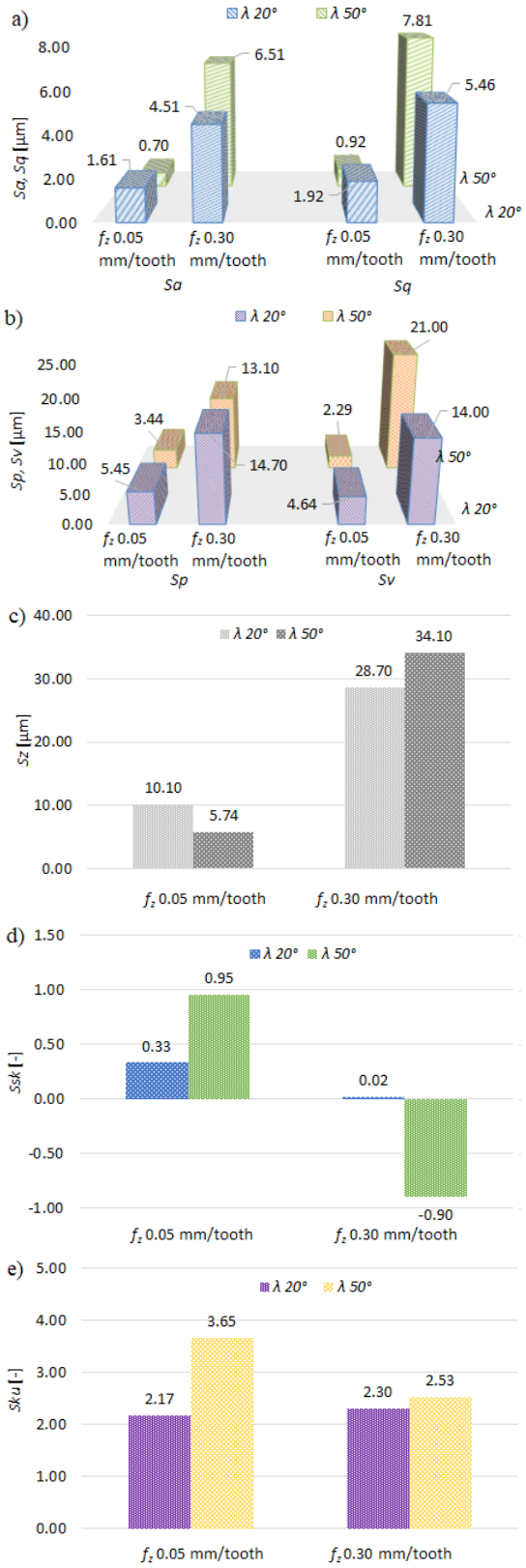

Fig. 6. *Feed per tooth and helix angle versus 3D surface roughness parameters: a) Sa, Sq, b) Sp, Sv, c) Sz, d) Ssk, e) Sku*

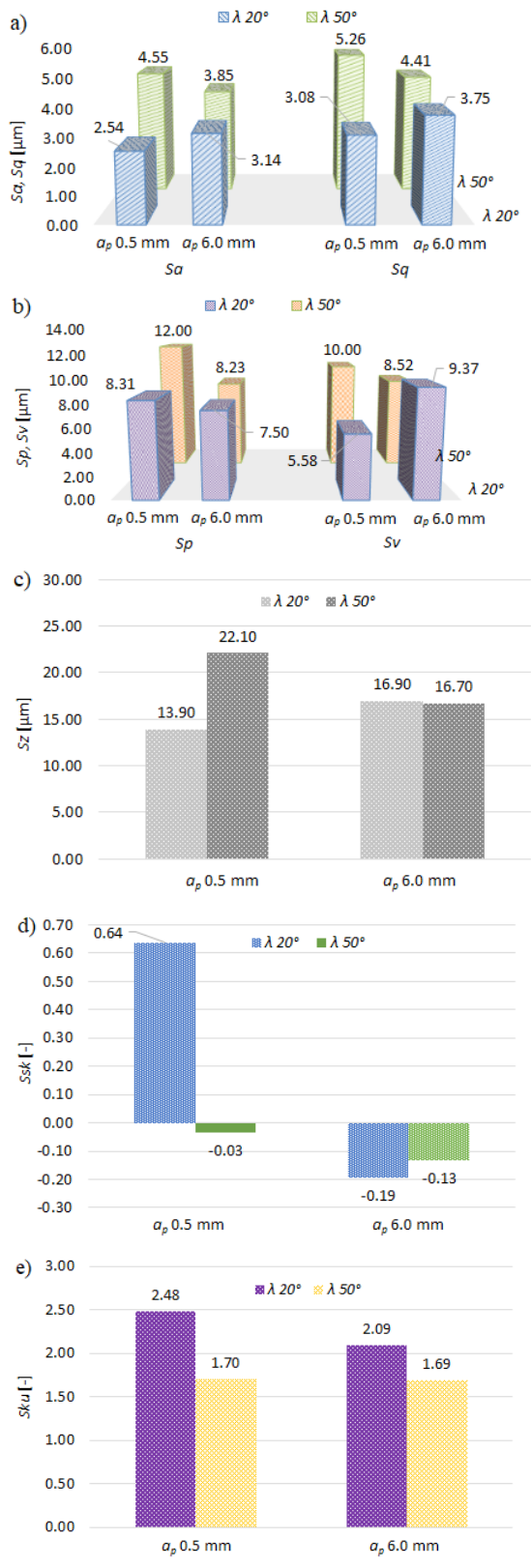

Fig. 7. *Axial depth of cut and helix angle versus 3D surface roughness parameters: a) Sa, Sq, b) Sp, Sv, c) Sz, d) Ssk, e) Sku*

a helix angle of 50°. For a_p equal to 6.0 mm, the *Sz* values are similar.

It can be observed that, in most cases, the Ssk parameter takes negative values (the higher frequency of deep valleys is defined as a plateau and is considered optimal). However, for the milling process conducted with a helix angle of 20° and a_p of 0.5 mm, this parameter takes a positive value. Moreover, the symmetric distribution of the profile is reflected by zero skewness (the value is similar to that observed for a_p 0.5 and λ 50°). The *Sku* parameter takes only positive values. These values decrease with increasing the axial depth of cut (for a helix angle of 20°) and remain on a similar level for a helix angle of 50°.

2.3 Surface Topography Maps

For illustrative purposes and better insight, Fig. 8 presents examples of 3D surface topography maps obtained from the rough milling process for AZ31B magnesium alloy conducted with a cutting speed of 400 m/min, using all analysed cutting tools (with various rake and helix angles).

An analysis of the isometric images demonstrates that all 3D surfaces have a typical, heterogeneous structure. There are high peaks and deep valleys, and the machining marks are characteristic of the applied machining method. The surfaces machined with the use of all tools do not differ from each other to any significant extent; however, a greater ratio of valleys can be observed on the surface obtained with the end mill described by a rake angle γ of 30°. It can be seen that an increase in the rake angle causes an increase in the height of the peaks and the depth of the valley on the machined surface. Surfaces obtained from milling using tools with variable helix angles have a similar heterogeneous structure and texture. Similarly to the case of various rake angles, relatively high peaks and deep valleys can be observed on the specimen surface.

2.4 Abbott-Firestone Curves

This section presents all obtained Abbott-Firestone curves. The curves were shown for the rake angles of 5° (Fig. 9) and 30° (Fig. 10) and for the helix angles of 20° (Fig. 11) and 50° (Fig. 12). These curves were

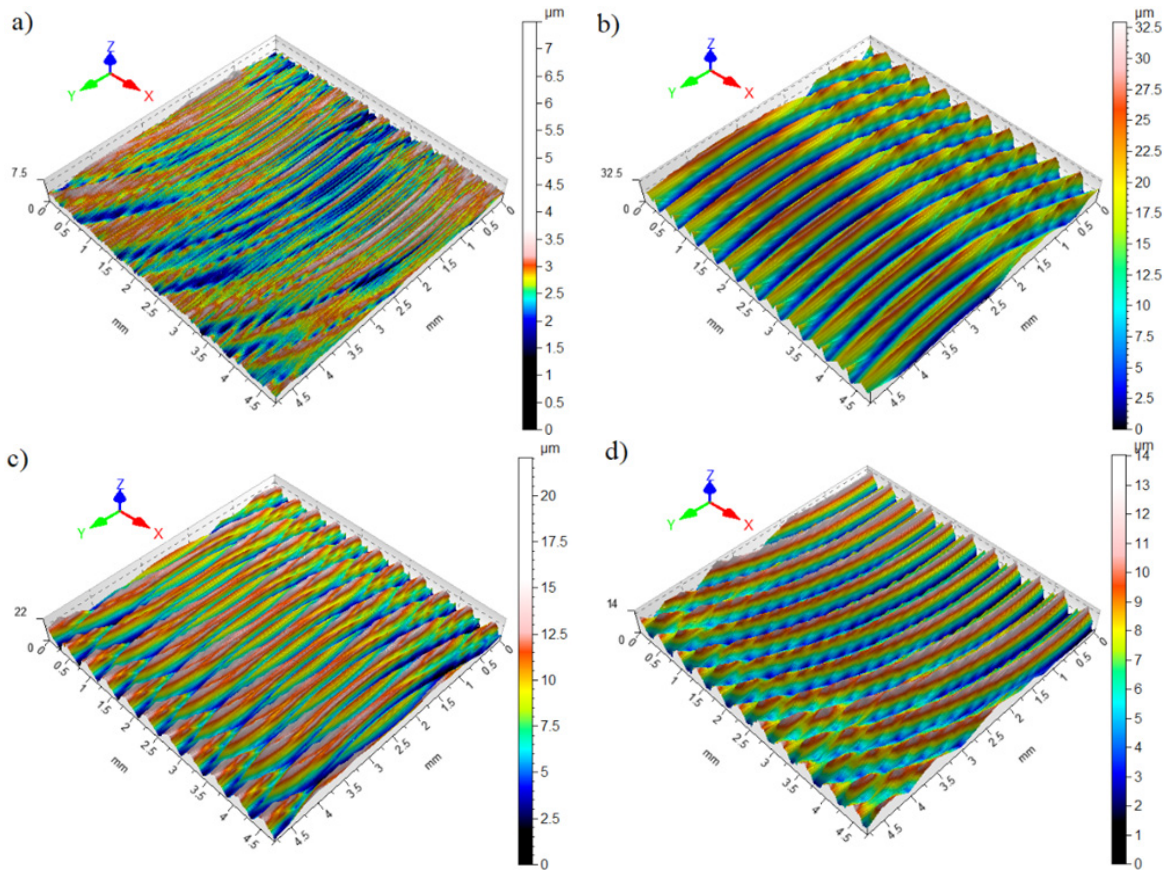

Fig. 8. *Surface topography maps: a) γ 5°, b) γ 30°, and c) λ_s 20°, d) λ_s 50° (v_c 400 m/min)*

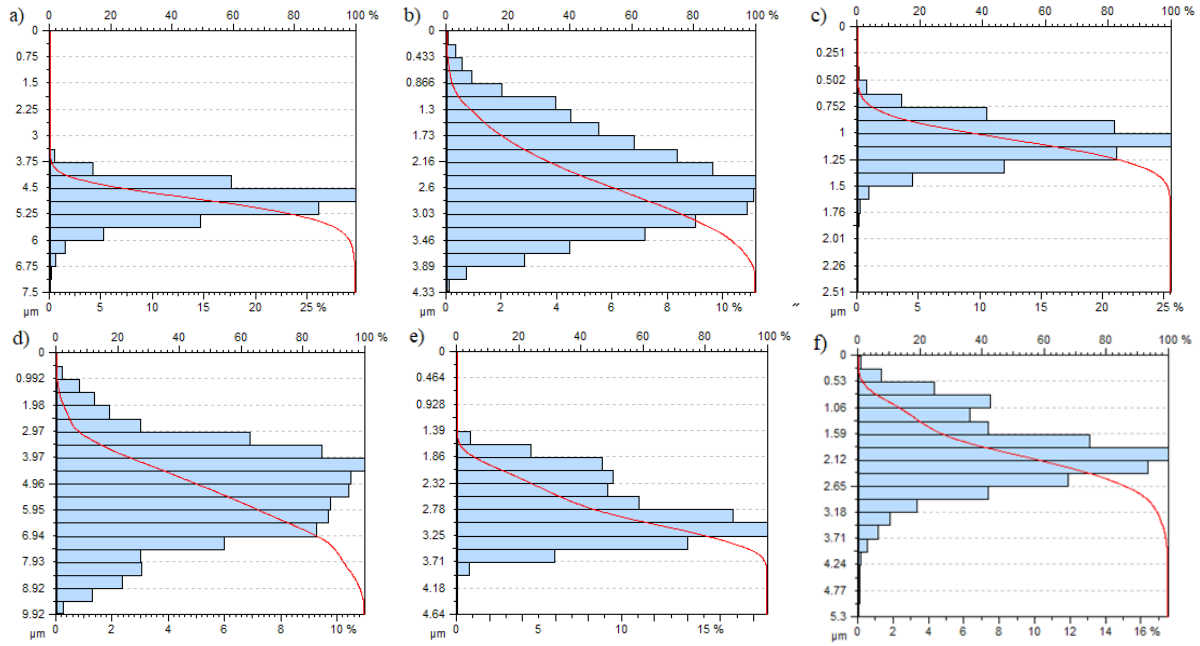

Fig. 9. *Abbott-Firestone curves obtained from milling a tool with a rake angle γ 5 °: a) v_c 400 m/min, b) v_c 1200 m/min, c) f_z 0.05 mm/tooth, d) f_z 0.30 mm/tooth, e) a_p 0.5 mm, and f) a_p 6.0 mm*

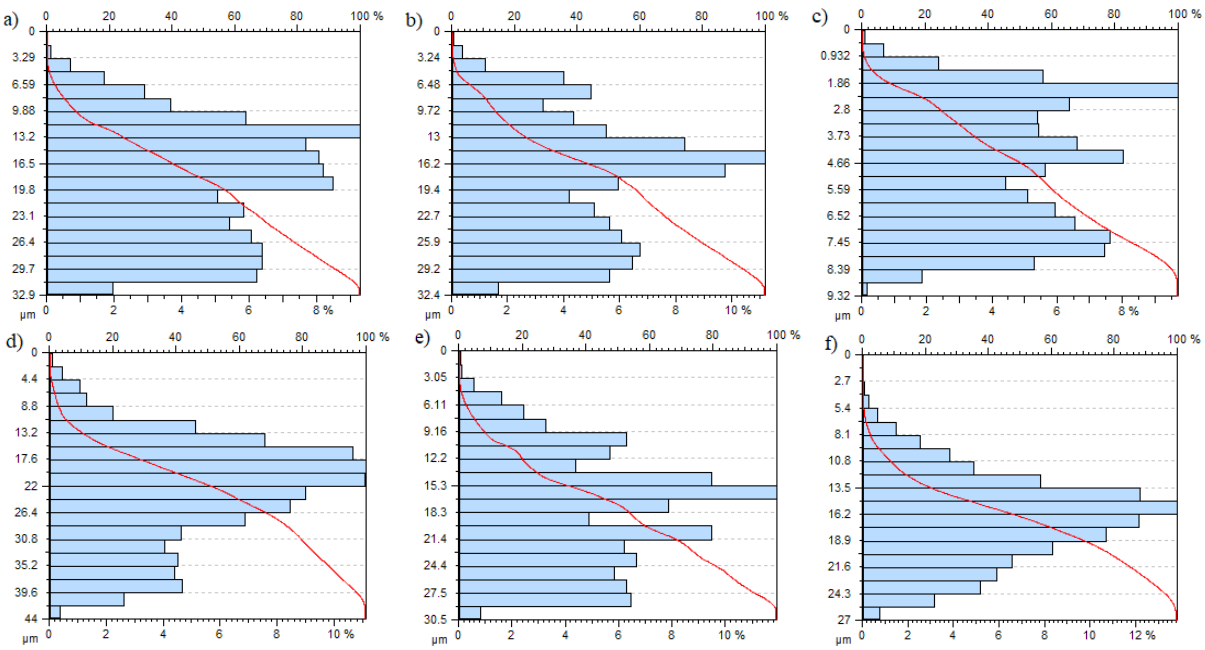

Fig. 10. *Abbott-Firestone curves obtained from milling a tool with a rake angle γ 30 °: a) v_c 400 m/min, b) v_c 1200 m/min, c) f_z 0.05 mm/tooth, d) f_z 0.30 mm/tooth, e) a_p 0.5 mm, and f) a_p 6.0 mm*

obtained for the milling process conducted with variable cutting speed, feed per tooth and axial depth of cut.

From the point of view of surface maintenance, the material ratio curves provide important information. The Abbott-Firestone curve can assume different shapes, the most favourable in terms of functional properties of the surface being the curves with a progressive or a progressive-degressive shape. Based on the shape of a material ratio curve, one can

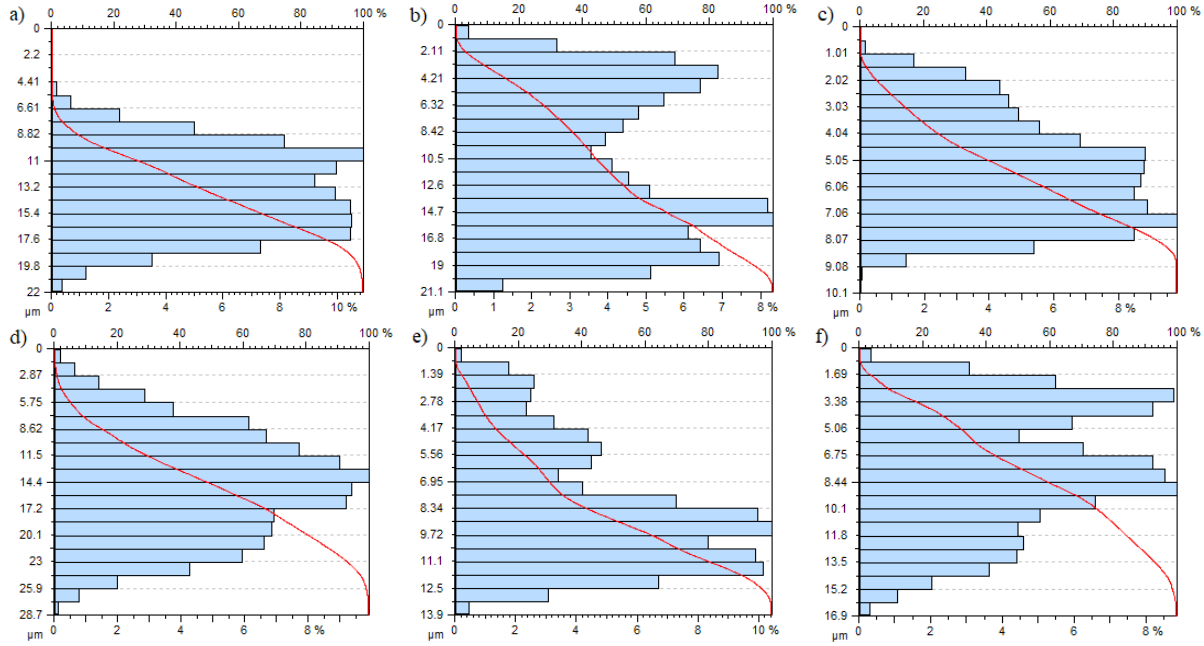

Fig. 11. *Abbott-Firestone curves obtained from milling a tool with a helix angle λ 20°: a) v_c 400 m/min, b) v_c 1200 m/min, c) f_z 0.05 mm/tooth, d) f_z 0.30 mm/tooth, e) a_p 0.5 mm, and f) ap 6.0 mm*

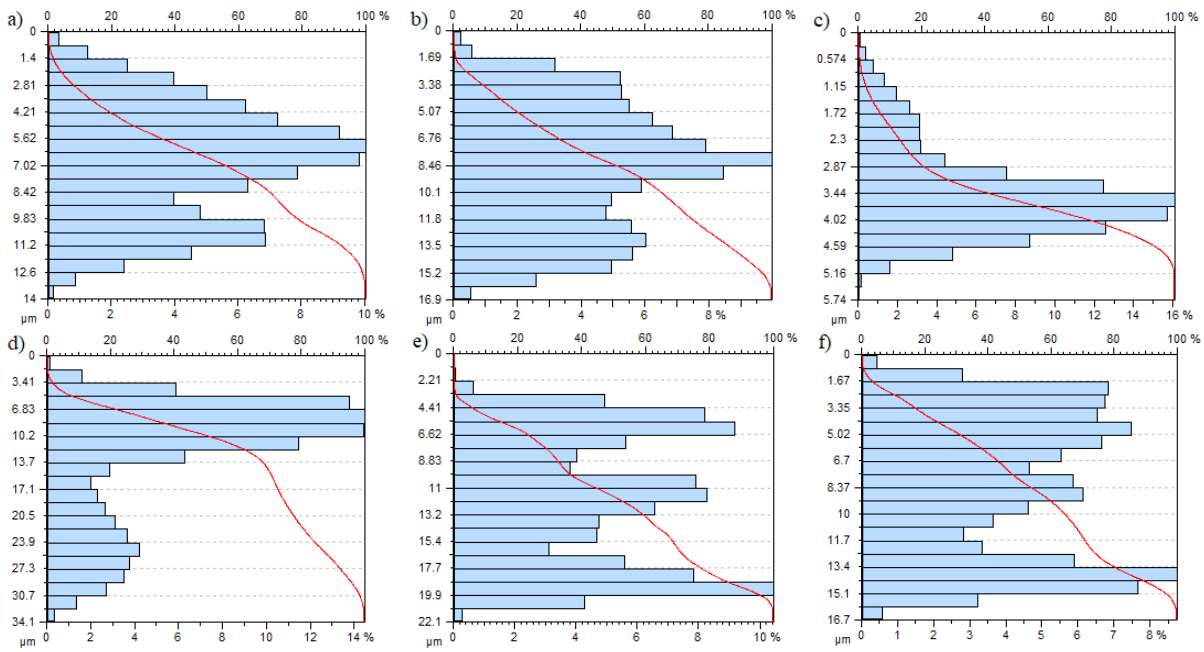

Fig. 12. *Abbott-Firestone curves obtained from milling a tool with a helix angle λ 50°: a) v_c 400 m/min, b) v_c 1200 m/min, c) f_z 0.05 mm/tooth, d) f_z 0.30 mm/tooth, e) a_p 0.5 mm, and f) a_p 6.0 mm*

draw inferences about, for example, the tribological wear resistance of a given surface. A progressive shape curve indicates that the analysed surface has rounded peaks and is more resistant to wear than the surface described by a degressive shape curve [30].

Fig. 9 shows the Abbott-Firestone curves for the tool with a rake angle of 5°. The curves have a degressive-progressive shape (mixed). A curve with the most uniform distribution of material share is obtained in the milling process conducted with a

cutting speed v_c 1200 m/min and a feed per tooth f_z 0.30 mm/tooth. It can, therefore, be concluded that the A-F curves have the desirable characteristics (owing to the rounded peaks and thus higher resistance to wear and friction) only in the so-called lower part of the material share curve.

Fig. 10 shows the Abbott-Firestone curves for the tool with a rake angle of 30°. The curves have approximately either a proportional or a degressive-progressive shape. Fig. 11 shows the Abbott-Firestone curves for the tool with a helix angle of 20°. In simple terms, the A-F curves have approximately a degressive-progressive shape. Fig. 12 shows the Abbott-Firestone curves for the tool with a helix angle of 50°. In simple terms, the A-F curves have approximately either a proportional or a degressive-progressive shape.

3 DISCUSSION

The results of this study investigating the rough milling of AZ31B magnesium alloy can be compared to some extent to the results reported in **[34]**, which studied the roughness of AZ91D/HP alloy after rough milling using the end mill with various rake angles, and in **[7]** and **[8]**, which described preliminary research on finish milling of AZ91D/HP and AZ31B magnesium alloys using the end mill with various helix angles.

A comparison of the results obtained from rough milling of magnesium alloys revealed that **[34]** an increase in cutting speed caused a decrease in roughness parameters while an increase in feed per tooth caused an increase in roughness parameters (*Ra*, *Rz*, *RSm*) on the lateral face of the workpiece. Similar relationships were also observed for roughness parameters (*Ra*, *Rq*, *RzDIN*, *Rt*, *Ry*, *RSm*) on the end face of the specimen. Lower roughness parameters were observed for the tool with a rake angle γ of 5°. For all tested technological parameters, the Ra parameter value was below 1.0 µm on the lateral face and approx. 1.5 µm on the end face of the specimen. A direct comparison of parameters, e.g. *Ra* and *Sa*, is quite troublesome; however, in the case of analysis, among others, for the *Ra* parameter, a similar tendency can be observed as for the *Sa* parameter. Smaller values of Sa were obtained when the tool with a smaller rake angle was used. This is due to the mutual relationship of these parameters; the *Ra* parameter was measured on the so-called sampling length (total measuring length lt = 4.8 mm, sampling length lr = 0.8 mm), while the Sa parameter was created from multiple repetitions of the measurement for the entire observed surface (scanning area 4.8 mm × 4.8 mm with 100 scanning steps).

Considerably lower values of the surface roughness parameters were reported in **[7]** and **[8]**. This resulted from the finish milling process being conducted under different conditions, i.e., with significantly smaller undeformed chip thickness or cross-section. It was found that to increase the stability of machining and to obtain a high surface finish, a more suitable tool for finishing milling was that with a helix angle of 20°. Like in the rough milling process, an increase in cutting speed led to a decreased surface roughness, while roughness parameters (*Ra*, *Rz*, *RSm*, *Rku*, *Rsk*) increased with feed per tooth. For variable v_c and f_z, the *Ra* parameter value was below approx. 1.0 µm on the lateral face and approx. 3.0 µm to 5.5 µm on the end face of the specimen, depending on the type of tool. A statistical analysis of *Ra* and *Rz* confirmed the inequality of the mean and median values for varying v_c. The statistical analysis results also showed that for all cases, the variations in f_z had an impact on the Ra parameter. Similar relationships were observed for other surface roughness parameters, i.e., *Rq*, *Rt*, *Rv* and *Rp*.

A comparison of the Abbott-Firestone curves demonstrates that for most studied cases of machining, e.g., in **[9]**, the curves have a degressive-progressive shape.

This research on rough milling of AZ31B focuses on 3D surface roughness parameters. For example, the Sa parameter value for the tool with γ 5° is below 1.0 µm for variable cutting speed, which indicates the high quality of the machined surface. The machining marks on the surface are characteristic of the milling process, with sharp peaks or deep valleys (typical heterogeneous structures). Although, for most cases, the Abbott-Firestone curves have a degressive-progressive shape that is typical of machining processes, some of these curves are distorted, taking on a proportional shape.

4 CONCLUSIONS

The results of this study lead to the following conclusions:

- 3D roughness parameters largely depend on the machining tool,
- better machining results and, hence lower surface roughness values were obtained when the milling process was conducted using the tools with a rake angle of 5° and a helix angle of 50°,
- regarding the tool with γ 5° and the *Sa* parameter, it was observed that with variables v_c and a_p, the

Sa value was below 1.0 µm while with variable f_z, it was below 2.0 µm,
- for the tool with λ_s 50°, the *Sa* value was below 4.0 µm for variable v_c, below 1.0 µm for f_z 0.05 mm/tooth, below 8.0 µm for f_z 0.30 mm/tooth, and below 6.0 µm for variable a_p,
- the *Sku* parameter takes only positive values which are predominantly below 3, which may prove that the peaks and grooves are rounded,
- an increase in cutting speed did not lead to any significant increase in surface roughness parameters for different rake angles; however, such an increase was observed for different helix angles,
- an increase in feed per tooth led to an increase in surface roughness parameters for the analysed tools,
- an increase in axial depth of cut did not cause any consistent trend in the change in surface roughness,
- the obtained 3D surface roughness maps show machining marks that are characteristic of rough milling, reflecting a typical heterogeneous structure with sharp peaks or deep valleys,
- the Abbott-Firestone curves are the easiest to interpret for the tool with γ 5° due to their degressive-progressive shape; the other curves have a distorted shape and hence are more difficult to interpret; nevertheless, their shape can approximately be described as proportional or degressive-progressive.

To provide more insight and further contribution to the development of mechanical engineering, future research should focus on investigating the parameters *Rvk*, *Rpk*, and *Rk* on Abbott-Firestone curves. Although the present study concludes, to some extent, the body of research on rough milling of magnesium alloys, studies can still be made on finish and precision milling as the two processes have not yet been thoroughly investigated. The present study was only conducted for the end face of the specimen. Further studies can be conducted for the lateral face of the specimen, particularly using tools with variable helix angles. In addition, studies can be conducted on rough, finish and precision milling of ultra-light alloys (both magnesium and aluminium alloys) containing lithium.

5 ACKNOWLEDGEMENTS

The project/research was financed with FD-20/IM-5/138.

6 REFERENCES

[1] Kuczmaszewski, J., Pieśko, P., Zawada-Michałowska, M. (2016.) Surface roughness of thin-walled components made of aluminium alloy EN AW-2024 following different milling strategies. *Advances in Science and Technology Research Journal*, vol. 10, no. 30, p. 150-158, **DOI:10.12913/22998624/62515**.

[2] Pradeep Kumar, M., Venkatesan, R., Manimurugan, M. (2022). Optimization of process parameters in turning of magnesium AZ91D alloy for better surface finish using genetic algorithm. *Acta Innovations*, vol. 43, p. 54-62, **DOI:10.32933/ActaInnovations.43.5**.

[3] Muralidharan, S., Karthikeyan, N., Kumar, A.B., Aatthisugan, I. (2017). A study on machinability characteristic in end milling of magnesium composite. *International Journal of Mechanical Engineering and Technology*, vol. 8, no. 6, p. 455-462.

[4] Ciecieląg, K. (2022). Study on the machinability of glass, carbon and aramid fiber reinforced plastics in drilling and secondary drilling operations. *Advances in Science and Technology Research Journal*, vol. 16, no. 2, p. 57-66. **DOI:10.12913/22998624/146079**.

[5] Matuszak, J. (2022). Comparative Analysis of the Effect of Machining with Wire and Ceramic Brushes on Selected Properties of the Surface Layer of EN AW-7075 Aluminium Alloy. *Advances in Science and Technology Research Journal*, vol. 16, no. 2, p. 50-56, **DOI:10.12913/22998624/146211**.

[6] Grzesik, W. (2015). Effect of the machine parts surface topography features on the machine service. *Mechanik*, vol. 8-9, p. 587-593, **DOI:10.17814/mechanik.2015.8-9.493**. (in Polish)

[7] Zagórski, I., Szczepaniak, A., Kulisz, M., Korpysa, J. (2022). Influence of the tool cutting edge helix angle on the surface roughness after finishing milling of magnesium alloys. *Materials*, vol. 15, no. 9, 3184, **DOI:10.3390/ma15093184**.

[8] Zagórski, I., Kulisz, M., Szczepaniak, A. (2024). Roughness parameters with statistical analysis and modelling using artificial neural networks after finish milling of magnesium alloys with different edge helix angle tools. *Strojniški vestnik - Journal of Mechanical Engineering*, vol. 70, no. 1-2, p. 27-41, **DOI:10.5545/sv-jme.2023.596**.

[9] Korpysa, J., Kuczmaszewski, J., Zagórski, I. (2023). Surface quality of AZ91D magnesium alloy after precision milling with coated tools. *Strojniški vestnik - Journal of Mechanical Engineering*, vol. 69, no. 11-12, p. 497-508, **DOI:10.5545/sv-jme.2023.651**.

[10] Sathyamoorthy, V., Deepan, S., Sathya Prasanth, S.P., Prabhu, L. (2017). Optimization of machining parameters for surface roughness in end milling of magnesium AM60 alloy. *Indian Journal of Science and Technology*, vol. 10, no. 32, p. 1-7, **DOI:10.17485/ijst/2017/v10i32/104651**.

[11] Zagórski, I., Korpysa, J. (2019). Surface quality in milling of AZ91D magnesium alloy. *Advances in Science and Technology Research Journal*, vol. 13, no. 2, p. 119-129, **DOI:10.12913/22998624/108547**.

[12] Alharti, N.H., Bingol, S., Abbas, A.T., Ragab, A.E., El-Danaf, E.A., Alharbi, H.F. (2017). Optimizing cutting conditions and prediction of surface roughness in face milling of AZ61 using

regression analysis and artificial neural network. *Advances in Materials Science and Engineering*, vol. 2017, no. 1, 7560468, **DOI:10.1155/2017/7560468**.

[13] Chirita, B., Grigoras, C., Tampu, C., Herghelegiu, E. (2019). Analysis of cutting forces and surface quality during face milling of a magnesium alloy. *IOP Conference Series: Materials Science and Engineering*, vol. 591, 012006, **DOI:10.1088/1757-899X/591/1/012006**.

[14] Ruslan, M.S., Othman, K., Ghani, J.A., Kassim, M.S., Haron, C.H. (2016). Surface roughness of magnesium alloy AZ91D in high speed milling. *Jurnal Teknologi*, vol. 78, no. 6-9, p. 115-119, **DOI:10.11113/jt.v78.9158**.

[15] Shi, K., Zhang, D., Ren, J., Yao, C., Huang, X. (2016). Effect of cutting parameters on machinability characteristics in milling of magnesium alloy with carbide tool. *Advances in Mechanical Engineering*, vol. 8, no. 1, **DOI:10.1177/1687814016628392**.

[16] Marakini, V., Pai, S., Bhat, U., Singh, D., Achar, B. (2022). High speed machining for enhancing the AZ91 magnesium alloy surface characteristics: Influence and optimisation of machining parameters. *Defence Science Journal*, vol. 72, no. 1, p. 105-113, **DOI:10.14429/dsj.72.17049**.

[17] Marakini, V., Pai, S., Bhat, A., Bangera, S. (2022). Surface integrity optimization in high speed milling of AZ91 magnesium alloy using TOPSIS considering vibration signals. *Materials Today: Proceedings*, vol. 52, p. 802-809, **DOI:10.1016/j.matpr.2021.10.154.**

[18] Jouini, N., Ruslan, M.S.M., Ghani, J.A., Haron, C.H.C. (2023). Sustainable high-speed milling of magnesium alloy AZ91D in dry and cryogenic conditions. *Sustainability*, vol. 15, no. 4, 3760, **DOI:10.3390/su15043760**.

[19] Kanan, M., Zahoor, S., Habib, M.S., Ehsan, S., Rehman, M., Shahzaib, M., Khan, S.A., Ali, H., Abusaq, Z., Hamdan, A. (2023). Analysis of carbon footprints and surface quality in green cutting environments for the milling of AZ31 magnesium alloy. *Sustainability*, vol. 15, no. 7, 6301, **DOI:10.3390/su15076301**.

[20] Gobivel, K., Vijay Sekar, K.S. (2022). Influence of cutting parameters on end milling of magnesium alloy AZ31B. *Materials Today: Proceedings*, vol. 62, p. 933-937, **DOI:10.1016/j.matpr.2022.04.075**.

[21] Kim, J.D., Lee, K.B. (2010). Surface Roughness Evaluation in dry-cutting of magnesium alloy by air pressure coolant. *Engineering*, vol. 2, no. 10, p. 788-792, **DOI:10.4236/eng.2010.210101**.

[22] Chhetri, S., Tariq, M., Mohapatra, S., Sumi, V., Zhimomi, A., Davis, R., Singh, A. (2020). Surface characteristics enhancement of biocompatible Mg alloy AZ31B by cryogenic milling. *IOP Conference Series: Materials Science and Engineering*, vol. 1004, 012011, **DOI:10.1088/1757-899X/1004/1/012011**.

[23] Sivam, S.P., Bhat, M.D., Natarajan, S., Chauhan, N. (2018). Analysis of residual stresses, thermal stresses, cutting forces and other output responses of face milling operation on ZE41 magnesium alloy. *International Journal of Modern Manufacturing Technologies*, vol. 10, no. 1, p. 92-101.

[24] Kumar, R., Katyal, P., Kumar, K. (2023). Effect of end milling process parameters and corrosion behaviour of ZE41A magnesium alloy using Taguchi based GRA. *Biointerface Research in Applied Chemistry*, vol. 13, no. 3, 214, **DOI:10.33263/briac133.214**.

[25] Guo, Y.B., Salahshoor, M. (2010). Process mechanics and surface integrity by high-speed dry milling of biodegradable magnesium-calcium implant alloys. *CIRP Annals - Manufacturing Technology*, vol. 59, no. 1, p. 151-154, **DOI:10.1016/j.cirp.2010.03.051**.

[26] Salahshoor, M., Guo, Y.B. (2011). Surface integrity of magnesium-calcium implants processed by synergistic dry cutting-finish burnishing. *Procedia Engineering*, vol. 19, p. 288-293, **DOI:10.1016/j.proeng.2011.11.114**.

[27] Salahshoor, M., Guo, Y.B. (2011). Cutting mechanics in high speed dry machining of biomedical magnesium-calcium alloy using internal state variable plasticity model. *International Journal of Machine Tools & Manufacture*, vol. 51, no. 7-8, p. 579-590, **DOI:10.1016/j.ijmachtools.2011.04.004**.

[28] Qiao, Y., Wang, S., Guo, P., Yang, X., Wang, Y. (2018). Experimental research on surface roughness of milling medical magnesium alloy. *IOP Conference Series: Materials Science and Engineering*, vol. 397, 012114, **DOI:10.1088/1757-899X/397/1/012114**.

[29] Desai, S., Malvade, N., Pawade, R., Warhatkar, H. (2017). Effect of high speed dry machining on surface integrity and biodegradability of Mg-Ca1.0 biodegradable alloy. Materials Today: Proceedings, vol. 4, no. 6, p. 6817-6727, **DOI:10.1016/j.matpr.2017.06.447**.

[30] Skoczylas, A., Kłonica, M. (2023). Selected properties of the surface layer of C45 steel samples after slide burnishing. *Materials*, vol. 16, no. 19, 6513, **DOI:10.3390/ma16196513**.

[31] Pawlus, P., Reizer, R., Wieczorowski, M. (2021). Functional importance of surface texture parameters. *Materials*, vol. 14, no. 18, 5326, **DOI:10.3390/ma14185326**.

[32] Sedlaček, M., Gregorčič, P., Podgornik, B. (2017). Use of the roughness parameters Ssk and Sku to control friction - a method for designing surface texturing. *Tribology Transactions*, vol. 60, no. 2, p. 260-266, **DOI:10.1080/10402004.2016.1159358**.

[33] ISO 21940-11:2016. *Mechanical Vibration-Rotor Balancing-Part 11: Procedures and Tolerances for Rotors with Rigid Behavior*. International Organization for Standardization. Geneva

[34] Gziut, O., Kuczmaszewski, J., Zagórski, I. (2015). Surface quality assessment following high performance cutting of AZ91HP magnesium alloy. *Management and Production Engineering Review*, vol. 6, no. 1, p. 4-9, **DOI:10.1515/mper-2015-0001**.